Tapiador, M., Escobar Vera, C., Soriano Amat, M., Martín López, S., González Herráez, M., Hernández, A. & Fernández Ruiz, M.R. 2023, "Definition of a FPGA-based SoC architecture for PRBS transmission in optical spectroscopy", IEEE Transactions on Instrumentation and Measurement, vol. 72, art. no. 2007109, pp. 1-9.

Available at https://dx.doi.org/10.1109/TIM.2023.3315366

Definition of a FPGA-based SoC Architecture for PRBS Transmission in Optical Spectroscopy

Miguel Tapiador, Camilo Escobar-Vera, Miguel Soriano-Amat, Sonia Martin-Lopez, *Member, IEEE*, Miguel Gonzalez-Herraez, *Senior Member, IEEE*, Álvaro Hernández, *Senior Member, IEEE*, and María R. Fernández-Ruiz

***Abstract*—Optical spectroscopy is a well-known tool typically employed for characterizing the properties of materials by analyzing their iteration with light. One of the most spread techniques is the dual comb spectroscopy, since it accomplishes ultra-high resolution, and high sensitivity measurements with a relatively simple platform including a single, relatively narrow-band photodetector. The employed optical dual comb can be implemented through electro-optical (EO) modulation driven by pseudo-ransom binary sequences (PRBS) at high data rates, commonly in the range of tens of Gbps. For that purpose, the run-time generation and transmission of adaptive PRBS is still an open challenge, often involving expensive and not flexible high-speed digital systems, with a few commercially available solutions that sometimes do not match the application requirements efficiently. In this context, this work describes the definition and implementation of a System-on-Chip (SoC) architecture, based on a FPGA device, capable of generating and transmitting two PRBS for a dual comb, at a data rate up to 5 Gbps. The architecture can be configured and its operation modified in run time, thanks to the general-purpose processor involved, in charge of managing an Ethernet link to receive new PRBS to be transmitted or set up certain parameters. The proposed design has been validated experimentally on a dual comb spectroscopy measurement, where the absorption of a hydrogen cyanide (HCN) gas cell has been successfully characterized.**

***Index Terms*—Optical spectroscopy, Dual comb, System-on-Chip, FPGA**

This work was supported in part by the MCIN/AEI/ 10.13039/501100011033 and by European Union NextGenerationEU/PRTR (POM project, ref. PID2019-105470RA-C33, and ALONE project, ref. TED2021-131773B-I00), in part by Comunidad de Madrid and Feder Program under grant SINFOTON2-CM: S2018/NMT-4326, in part by the Spanish MCIN/AEI/10.13039/501100011033 and the European Union NextGenerationEU/PRTR under Grants PSI ref. PLEC2021-007875, and TREMORS ref. CPP2021-008869, in part by the Spanish MCIN/AEI/10.13039/501100011033 and FEDER under grant PID2021-128000OB-C22, in part by the European Innovation Council under Grant SAFE: ref. 101098992. The work of MRFR was supported by the MCIN/AEI/10.13039/501100011033 and European Union NextGenerationEU/PRTR under grant RYC2021-032167-I. The work of MSA was supported by MCIN/AEI/10.13039/ 501100011033 and the FSE under grant PRE-2019-087444.

Miguel Tapiador, Camilo Escobar-Vera, Miguel Soriano-Amat, Sonia Martin-Lopez, Miguel Gonzalez-Herraez, Álvaro Hernández and María R. Fernández-Ruiz are with the Universidad de Alcalá, Electronics Department, 28801 Alcalá de Henares (Madrid), Spain (e-mail: miguel.tapiador@edu.uah.es).

I. Introduction

Optical spectroscopy is a long-established field that allows for the observation and study of the fundamental properties of materials by analyzing the iteration between light and matter. There exists a wide panoply of spectroscopy techniques, which are mainly based on measuring absorption, emission, scattering or rotation of light by atoms or molecules [1-4]. One of the more widespread approach is the absorption spectroscopy [5-7]. This method compares the power of a light beam before and after the interaction with a sample of interest in a frequency-resolved fashion. Atoms and molecules can be identified by which frequencies of light they absorb, thus revealing the energy structure and the composition of matter. The advent of optical frequency combs (OFC) was an important step forward the establishment of highly precision spectroscopy, as they provide a broad and uniformly spaced modal structure with unmatched frequency accuracy [8, 9]. However, spectrally resolving the comb lines is a challenging task that imposes the need for broadband detectors and fast response instrumentation.

Dual comb spectroscopy arose as a solution to efficiently resolve all the spectral lines of a broadband source with a single photodetector while maintaining the frequency accuracy and spectral resolution, and allowing for long interrogation paths with high sensitivity [10, 11]. This approach relies on the use of a dual frequency comb (DFC), i.e., a pair of identical OFC with slightly different repetition rate. Either one or both combs travel through the sample, depending on whether the detection of the magnitude and phase or simply the magnitude of the absorption peak are targeted in the procedure, respectively. In the former case, the second comb is used as a reference (or local oscillator, LO). Then, the combs are mixed and detected in a single photodetector. The beating between the two combs produces an efficient downconversion of the sampled optical spectral response to the radio-frequency (RF) domain, which can readily accessible with RF electronics.

This approach employed in dual comb spectroscopy has been extended into a broad variety of fields, which now leverage DFC to perform broadband measurement with excellent frequency resolution and high energy efficiency, while keeping simple detection and acquisition stages. Manifest examples of technologies employing DFC are LIDAR (Light

Detection and Ranging) [12, 13], ranging [14], vibrometry [15], metrology [16], waveform characterization [17], distributed fiber-optic sensing [18, 19] or imaging [20], among others.

In the literature, one can find a wide variety of approaches for generating DFC. The original implementation used stabilized mode-locked lases [8]. Yet, DFC generation has been progressively conducted with a variety of platforms [9, 21-23]. Among them, electro-optic (EO) frequency comb generation has arisen as an attractive solution for applications in the near infrared (IR) band. The main reasons are the high flexibility in the selection of the comb's line spacing and number of lines, the high power per comb line attainable and the intrinsic mutually coherence between combs, as both are commonly generated from the same laser source [24-26]. In this approach, a continuous-wave (CW) optical signal seeds two branches with an EO intensity or phase modulator (or a combination of both), which is driven by a RF signal. Different driving signals are used as a function of the desired comb's parameters, e.g., sinusoidal signals at the target repetition rate or arbitrary periodic sequences whose magnitude spectral envelope is as smooth as possible. The former attains wider bandwidths although is limited to few (100-150) lines [21]. In contrast, when using ad-hoc periodic sequences, the bandwidth is limited to tens of GHz (as imposed by the RF signal generator and/or the RF and EO components), although combs with tens of thousands lines have been demonstrated [26]. Amongst the periodic sequences employed to implement frequency combs, maximum-length pseudo-random binary sequences (PRBS) stand out for their excellent periodic autocorrelation properties [27-29] and for the flatness of their magnitude spectral envelope.

Commercially available PRBS generators nowadays are simple chips allowing for tens of Gbps data rates, but generally including just certain values for the sequence code length. Very often, those values are PRBS-7, 15, 20 or 31, which are the typically employed in bit error data rate measurement in telecom. However, in spectroscopy, code length tunability is highly desired, as it imposes the frequency resolution of the measurement (as detailed in the following section). Additionally, the selection of the repetition rate of the two combs in an independent fashion and with high accuracy (i.e., in the Hz range), while maintaining a common reference clock, is critical for a proper adjustment of the downconversion operation. Note that the need for a common reference clock is fundamental for enhancing the mutual temporal coherence between combs. Arbitrary waveform generators (AWG) or pulse pattern generators offering high tunabiliy in the PRBS length selection and combs' repetition rate over Gbps bit rates are typically bulky and expensive. Hence, the generation of a maximum-length PRBS with possibility to arbitrary select the parameters of the produced combs and with a compact and low-cost setup remains a challenging endeavor.

Apart from those previous works based on commercially available PRBS generators [26] [30] with scarce flexibility, FPGA (Field-Programmable Gate Array) devices have already been used in the generation and transmissions of PRBS at high bit rates [31]. In [29], in dual comb spectroscopy, a Xilinx Virtex7 FPGA is dedicated to transmit 511 bits long sequences at rates up to 10 Gbps, by means of the specialized serial transceivers existing in the die. Nevertheless, the PRBS sequences are generated offline and loaded in the board, so it seems not to support any further flexibility or run-time reconfiguration options. Furthermore, no details are provided about the hardware architecture.

In this context, this work presents a System-on-Chip (SoC) architecture, based on a FPGA device, capable of generating a user-defined DFC based on maximum length PRBS sequences with high flexibility in the selection of the combs' parameters while ensuring mutual coherence. Our solution generates arbitrary length PRBS with 5 Gbps data rate in a compact and embeddable device. The proposed architecture is experimentally validated in an EO dual comb spectroscopy measurement where the absorption of a hydrogen cyanide (HCN) gas cell has been characterized. The main contributions of this work can be summarized as follows:

- The definition and implementation of an efficient hardware architecture, capable of generating two PRBS sequences at rates up to 5 Gbps, with a slight rate difference in the range of hundreds of Hz.
- The architecture involves a general-purpose processor, in charge of managing an Ethernet connection that is used to modify and configure the PRBS sequences and their transmissions in run time, thus achieving a degree of tunability not reported in previous works to our best knowledge.
- This approach provides a flexible solution for a wide range of optical equipment, where the capability to transmit PRBS sequences at high data rates is a key feature to achieve the expected performance in many communications or instrumentation applications. In this way, the proposal has been successfully validated hereinafter in a spectroscopy experimental setup.

The rest of the manuscript is organized as follows: Section II provides a general description of the proposal; Section III details the SoC architecture defined for the configurable transmission of PRBS; Section IV deals with some experimental results in optical spectroscopy; and, finally, conclusions are discussed in Section V.

II. General Description of the System

As previously introduced, dual comb spectroscopy employs a pair of mutually stabilized optical frequency combs with slightly different line spacing. When generating the optical combs via EO modulation driven by a PRBS of code length k (PRBS-k), the magnitude of the spectral response has a smooth, sinc-like envelope centered around the carrier frequency f_{opt}. To avoid an ambiguous downcoversion of the beating pair of lines at both sides of f_{opt}, one of the combs is frequency shifted, up to guarantee that each pair of probe-LO neighboring lines beats at a different RF frequency (see Fig. 1.a). This is attained by using an acousto-optical frequency shifter (AOFS), whereas the secondary lobes of the sinc-like spectrum are filtered out by

means of an optical band-pass filter. Within the remaining bandwidth B_o, we have approximately $N = 2^{k+1} - 3$ lines. Considering the effect of the AOFS and of the band-pass filter, we can model the two combs composing the dual frequency comb as follows,

$$E_{pb}(f) = \sum_{m=0}^{N} A_m \cdot e^{j\phi_m} \cdot \delta(f - \upsilon_m), \quad (1)$$

$$E_{LO}(f) = \sum_{m=0}^{N} A'_m \cdot e^{j\phi'_m} \cdot \delta(f - \upsilon'_m), \quad (2)$$

where $E_{pb}(f)$ and $E_{LO}(f)$ are the frequency-domain representation of the probe and LO combs, respectively; A_m, υ_m, ϕ_m, A'_m, υ'_m, and ϕ'_m are the amplitude, frequency and phase of the m-th comb line of the probe and the LO, respectively. The frequency of each line can be written in term of the repletion rate, f_R, as $\upsilon_m^{(\prime)} = \upsilon_0^{(\prime)} + m \cdot f_R^{(\prime)}$. The difference in the frequency of the first comb line of each comb line is imposed by the AOFS, i.e., $\upsilon_0 = \upsilon_0' + f_{AOFS}$. More details about the value of f_{AOFS} to be selected for a proper conditioning of the spectrometer is given in Section IV. The probe comb, with line spacing $f_R = B_o/(N-1)$, is sent through the sample of interest. Assuming that the spectral response of the sample is $H_s(f) = |H_s(f)| \cdot exp\{j \cdot \phi_s(f)\}$, the probe spectrum at the output of the sample is,

$$E_s(f) = \sum_{m=0}^{N} A_m |H_S(\upsilon_m)| e^{j(\phi_m + \phi_s(\upsilon_m))} \cdot \delta(f - \upsilon_m), \quad (3)$$

i.e., the probe spectrally samples the sample spectral response at frequencies υ_m. The second comb, with line spacing $f'_R = f_R + \delta f$ (with $\delta f \ll f_R$, being the mismatch between line spacing of the two OFC), is used as local oscillator (Fig. 1.a). The LO comb has the same number of lines as the probe one, resulting in a bandwidth of $B'_o = B_o + N \cdot \delta f$. The two combs are mixed and photodetected. Upon detection, the lines of the probe and LO combs beat into the RF domain, producing clusters of beating lines around multiples of f_R. By filtering the RF lines corresponding to the beating of neighboring lines, an RF comb (with line spacing δf), containing the full spectral information of the sample (i.e., its magnitude and phase spectral response), is finally obtained (Fig. 1.b) according to (4),

$$V(f) = \sum_{m=0}^{N} A_m A'_m |H_S(\upsilon_m)| e^{j(\phi_m + \phi_s(\upsilon_m) - \phi'_m)} \cdot \delta(f - \nu_m^{RF}), \quad (4)$$

where $\upsilon_m^{RF} = (\upsilon_0 - \upsilon'_0) + m \cdot \delta f$. To avoid any aliasing of lines in the RF domain, the line spacing offset between combs must meet that

$$\delta f < \frac{f_R}{2 \cdot N}. \quad (5)$$

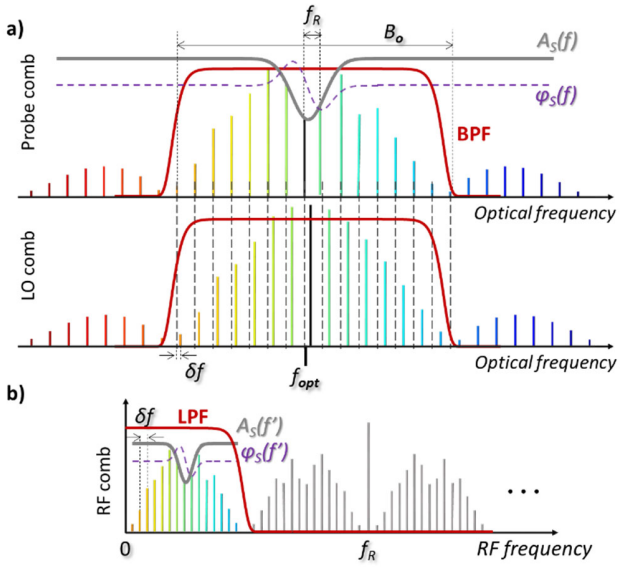

Fig. 1. Dual comb spectroscopy concept. a) An optical frequency comb passes through a sample of interest. This comb samples the absorption features of the sample in magnitude $A_s(f)$ and phase $\varphi_s(f)$. A second comb identical to the first one, but with a slight difference of δf in the line spacing, is used as a reference. To avoid unambiguous downconversion, the main lobe of the sinc-like spectral envelope is filtered by an optical band pass filter (BPF), whereas one of the combs is conveniently frequency shifted. The combs are then mixed and detected. b) The resulting signal is low-pass filtered (LPF) to keep a comb at RF frequencies containing the complex-envelope information of the absorption feature over a compressed frequency axis.

When a PRBS is employed to generate OFC, each comb line has a different instantaneous phase. Still, if the same binary sequence is employed in both the probe and LO combs, $\phi_m = \phi'_m$, such spectral phase is compensated upon photodetection, directly obtaining the spectral response of the sample. This can be readily determined by noting that the detected RF comb lines are proportional to the product of the electric field of the probe and the conjugated LO neighboring lines. In contrast with other approaches producing transform-limited combs (i.e., in which all lines maintain the same phase, corresponding with a train of transform-limited short pulses in time domain), PRBS considerably increases the signal-to-noise ratio of the system. In particular, a transform-limited comb has a peak-to-average power ratio (PAPR) equal to the inverse of the duty cycle from the pulse train, or equivalently, equal to the number N of generated lines,

$$PAPR = \frac{P_p}{P_{avg}} = \frac{B_o}{f_R} = N, \quad (6)$$

where P_p and P_{avg} are the peak and average powers of the train of pulses. In this case, to increase the power per line of the comb, the only solution is to increase the pulse peak power. However, in a fiber-based configuration, the maximum peak

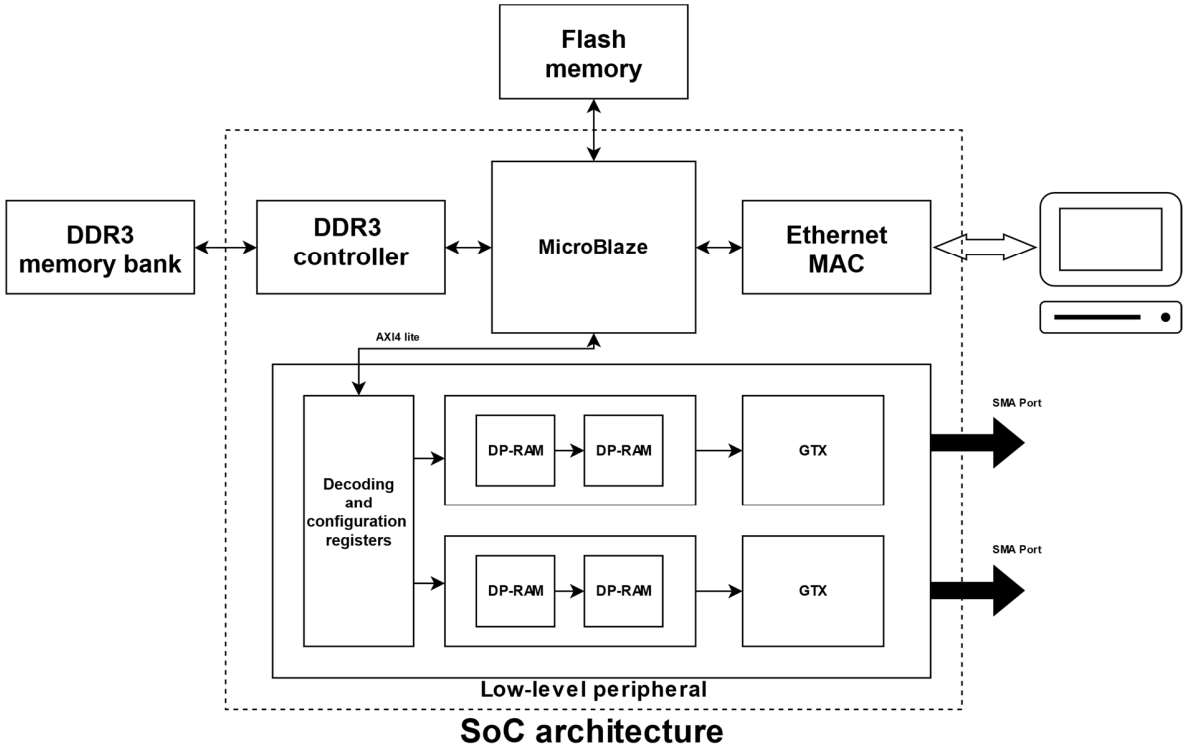

Fig. 2. General block diagram of the proposed SoC architecture.

power is limited by the onset of nonlinear effects. A PRBS sequence has a PAPR of about 2, since the period of the sequence has practically the same number of ones and zeros. A PAPR closest to the optimal value of 1 is highly desired, since, if the power of the signal is spread along the period, such signal can be amplified without the onset of nonlinear effects along the optical path. This approach allows a considerable increase of power per comb line and, therefore, of the SNR.

A highly flexible maximum-length PRBS generator based on a SoC architecture is here designed and employed for the implementation of a low-cost and massively deployable electro-optical dual comb spectroscopy scheme. For the sake of validation, such scheme is employed to measure the transmission through a $H^{13}C^{14}N$ gas cell (from Wavelength References), with a pressure of 3.3 kPa and a length of 5.5 cm. According to the data provided by the National Institute of Standards and Technology (NIST) [32], the HCN has an absorption peak at 1545 nm, which can be readily measured using conventional C-band optical components. The absorption peak has a full width at half maximum of approximately 1 GHz. For a proper characterization of the transmission of such sample, we require an optical frequency comb with a minimum bandwidth of 5 GHz. As previously mentioned, the number of bits of the employed PRBS will impose the frequency resolution of the spectroscopic measurement. For a frequency resolution in the MHz regime, we select a PRBS-10, having 2045 lines in the optical domain. The line spacing of the probe comb is then 2.446184 MHz. With such values, the offset between the comb lines is limited to 598 Hz, according to (5). In this case, we select $\delta f = 500$ Hz. Hence, we can resolve all the comb lines by simply using a single photodetector of a few MHz bandwidth (in our case, a photodetector of 100 MHz with a low-pass RF filter of 5 MHz was used). The LO comb must be generated with a bandwidth $B'_0 = 5.0010225$ GHz. Besides, both RF combs must be generated with a common clock reference, aimed at reducing RF frequency noise and increasing the mutual stability of both combs. A DFC with such features is implemented by employing the SoC architecture described in the following section.

III. System-on-Chip Architecture

The proposed FPGA-based SoC architecture consists of a Microblaze processor [33] and a specific low-level peripheral in charge of managing the PRBS sequences and their subsequent transmission at frequencies in the GHz range, as can be observed in Fig. 2. The Microblaze processor is responsible for the Ethernet link that allows to manage and configure the operation of the system in run time, including the PRBS sequences to be transmitted and some parameters, such as amplitude and operation frequency. In that way, the processor decodes and processes the information received from an external PC, and then downloads the corresponding configuration as 32-bit unsigned integers to the peripheral implemented in the programmable logic (PL). The latter is carried out by using the AXI (advanced extensible interface) protocol and a set of dual-port (DP) RAM memories, also depicted in Fig. 2. The Ethernet link presents a server-client architecture, where the Microblaze processor plays the role of server.

On the other hand, the most important element for the generation of digital sequences with frequencies in the range of

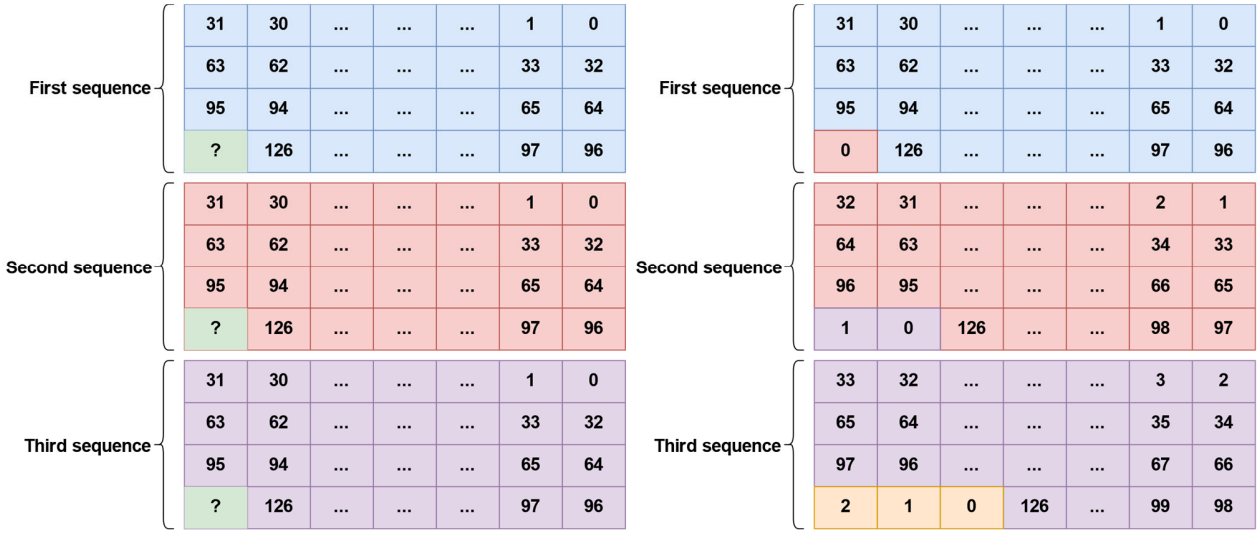

Fig. 3. Management of the blank bit to keep the optimal correlation function of the PRBS sequences in continuous transmissions.

GHz is the Multi-Gigabit Transceiver (MGT), available in FPGA devices from Xilinx, Inc. Particularly, this design is based on GTX modules [34], capable of reaching speeds of up to 6.6 Gbps. Since these blocks are integrated within the FPGA die, a peripheral on the PL has been proposed to encapsulate and configure them. One of the main limitations of the system is coming from the internal principle of operation from the GTX. This generates digital signals by serializing bit packets with a size M at a frequency f_o=M·f_{CLK}, where f_{CLK} is the clock frequency provided to the GTX by the PL design. In this case, the system has been configured to work with M=32 bits, so if the bit rate of the digital signal to be generated is f_o=5 Gbps, the clock to be supplied to the transceiver will have f_{CLK}=156.25 MHz. The drawback derived from this is that the generated digital signals have a length that is multiple of M=32, a condition not fulfilled in the case of PRBS-k sequences, which have a length of $(2^k - 1)$ bits. Considering that the sequences are sent to the transceiver in 32-bit packets, there will always be one blank bit at the end of each sequence. For example, in the case of a PRBS-7 (127 bits long), four 32-bit packets (128 bits) will be stored into the dual-port memories and sent to the transceiver. With this new blank bit, the continuous transmission of the PRBS signal is still periodic, but it degrades its autocorrelation performance. To deal with this issue, the proposed architecture implements a State Finite Machine (FSM) that eliminates the extra bit at the end of each transmission, so that the final digital signal generated corresponds to an exact PRBS. Fig. 3 shows a block diagram of this issue and the proposed approach to solve it.

A. Global SoC Operation

As shown in Fig. 2, the specific peripheral has been integrated into the SoC architecture together with a Microblaze processor, a DDR3 memory for instruction storage, a flash memory for the initial program startup, as well as different clock generators. The processor is responsible for the initialization of all the modules after the initial startup and for the initialization of the Ethernet server, which allows remote configuration and PRBS sequences downloading through an user interface.

After initial startup, the system is set with the last available configuration, while waiting for possible new sequences to be downloaded. Through the Ethernet link, the user can select the length k of the PRBS (from 7 to 15), the peak-to-peak amplitude m_{Vpp}, and the post-emphasis and pre-emphasis values (dBm) of the generated signals. Furthermore, the main output frequency f_o can also be set from 2 GHz to 5 GHz in steps of 200 MHz. On the other hand, the secondary sequence frequency f_{o2} is externally sourced, so its frequency may be manually varied.

After the user sends both configuration parameters and PRBS sequences to the system via Ethernet, the Microblaze processor decodes and downloads it to the peripheral via the AXI bus. While the configuration parameters are written in the corresponding internal registers in the peripheral, a new PRBS sequence is stored in the first dual-port RAM shown in Fig. 2. Since the length k of the sequence is one of the aforementioned configuration parameters, if the whole set of samples has been stored in the dual-port memory, the state machine comes into operation, transferring all the samples from the first memory to the second one, changing from the master clock domain in the peripheral to the clock domain of the corresponding transceiver. Once all the samples have been transferred, the finite state machine (FSM) moves to the next state and starts sending data to the transceiver for the final PRBS digital generation and a memory feedback process. This process allows the memory to be rewritten after performing a bit shift on each reading, thus eliminating the extra blank bit at the end of each sequence for the next successive transmission, as depicted in Fig. 3. The FSM will remain in this feedback state indefinitely until a new sequence is received (regardless of its length).

In this feedback state, dedicated to discard the extra blank bit at the end of each PRBS sequence, if a new sample is read, a bit shift is applied by rewriting the sample in the previous

position in the dual-port memory, as shown in Fig. 3. Since the current and previous samples are necessary to carry out this process, there is a latency of three clock cycles, thus limiting a minimum sequence size of four 32-bit samples (PRBS-7). For this process to work properly, the initial PRBS sent to the processor and stored in RAM memory must contain on its last position the first bit of the sequence. Since the user interface manages the generation and segmentation of the PRBS sequences before transferring them through the Ethernet link, it is also in charge of including this last bit before.

Fig. 4 shows the flowchart describing the operation of the MicroBlaze processor, as well as the different tasks implemented in the designed peripheral, from the configuration of the transceivers and the generation of the PRBS sequences to their serialization through the SMA (SubMiniature version A) ports at Gbps data rates.

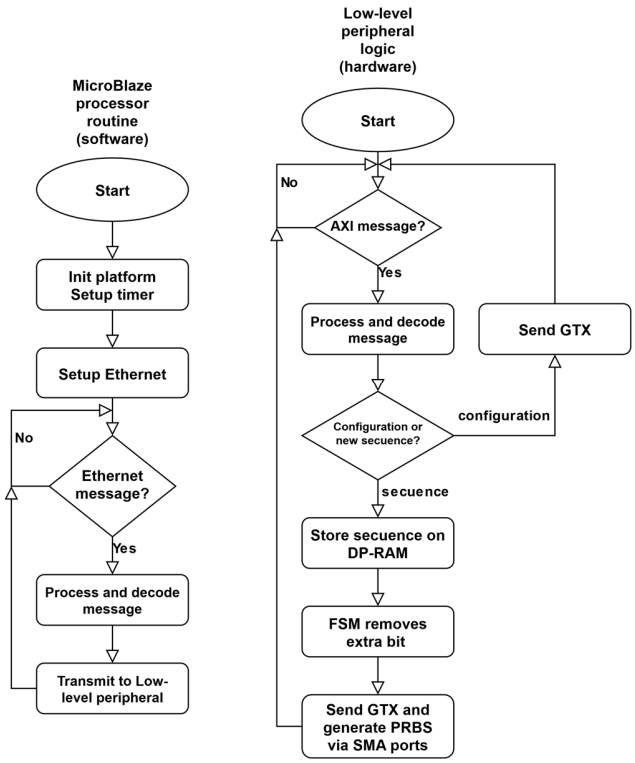

Fig. 4. Flowchart of the operation by the MicroBlaze processor and the proposed peripheral.

IV. Description of the Proposed Low-Level Peripheral

The PRBS sequences are generated as digital signals by the transceivers at a bit rate previously configured by the user. As already mentioned, a dedicated peripheral has been proposed to both control the transceivers and manage the sequences received from the processor by discarding the extra blank bit. Fig. 5 shows a block diagram of the internal architecture for the proposed peripheral. Since two equal sequences are generated but at slightly different output bit rates, each transceiver is managed independently. The control of every transceiver is based on two modules, one dedicated to its control and the other to the reception and management of the PRBS sequences. For that purpose, two successive dual-port memories are arranged for its transceiver, with a size of 1Kx32 bits (enough to store a complete PRBS-15). It is worth noting that longer sequences than PRSB-15 may be admitted by enlarging these dual-port memories. The first dual-port memory supports data to be transferred from the master clock domain into the transceiver clock one, whereas the second one allows the extra blank bit to be discarded.

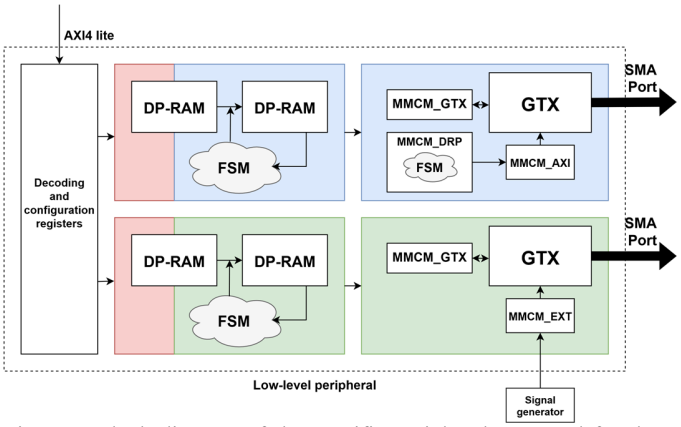

Fig. 5. Block diagram of the specific peripheral proposed for the transmission of the PRBS at GHz rates.

With regard to the different clock domains, the proposed peripheral has up to three clock domains. The first one is the master clock, coming from the AXI4-lite bus at a frequency of 100 MHz. It is generated from the external 200 MHz oscillator and controlled by the Microblaze processor. This clock handles the processor-peripheral AXI communication and, therefore, the corresponding writing of the PRBS samples in the first dual-port memory. On the other hand, the second and third clock domains are associated to the main transceiver and to the secondary one, respectively. Since the goal is the generation of a dual frequency comb, the mismatch in the repetition frequency of the two combs is to be generated by having two clock domains operating at different frequencies. Due to the constraints determined by the FPGA board used for the experimental tests, and described in detail later, only the secondary transceiver has an external clock source, whereas the main one has an internal clock source derived from the 100 MHz AXI bus clock. In order to allow the modification of both the transmitted sequences and their bit rate in run time, the proposed architecture implements a module that reconfigures the internal PLL (MMCM, Mixed-Mode Clock Manager) [35], which generates the second clock for the main transceiver from the AXI clock. On the other hand, the external clock source for the secondary transceiver can be manually set by the user.

As for the GTX blocks (the main and the secondary one), these modules instantiate both the transceiver core itself and other modules associated with it, such as clock signal buffers and a PLL (MMCM_GTX), whose function is to generate the different clocks needed by the core, with the exception of the clock initially supplied (see [33] for further information from

the manufacturer). The bit rate of the output digital signal depends on this clock. In the case of the external source for the secondary transceiver, the clock is received through a PLL (MMCM_EXT). Similarly, the internally generated clock for the main transceiver is also received by a PLL (MMCM_AXI), managed by the MMCM_DRP module [34] [35]. This module, which has been modified to generate up to 16 possible frequencies between 2 GHz and 5 GHz (in steps of 200 MHz), allows the internal PLL parameters to be configured in run time, as mentioned before.

IV. Experimental results

The SoC architecture described in the previous point has been implemented on the ML605 evaluation board from Xilinx Inc., which has a Virtex6 XC6VLX240T FPGA [36]. In this device, Table I shows the resource consumption of the architecture, both for the peripheral and the global system. As can be observed, the consumption of logic resources and RAM memory is low, so that the system can support extensions both in the implemented logic and in the length of the sequences to be transmitted.

TABLE I.
Resource consumption and percentage occupation of the global proposed architecture and the low-level peripheral

Resource	Low-level peripheral	Global architecture
Slice register	686 (~1%)	6725 (2%)
Slice LUT	930 (~1%)	7562 (5%)
IOB	4 (~1%)	76 (12%)
RAMB36E1	6 (2%)	16 (3%)
BUFG	12 (38%)	17 (53%)
DSP48E1	0 (0%)	3 (1%)
GTXE1	2 (10%)	2 (10%)
MMCM_ADV	4 (33%)	6 (50%)

Although the FPGA available in the aforementioned evaluation board has up to 20 transceivers, only one of these is directly connected to a SMA port in the board. Nevertheless, since the proposed architecture requires at least two GTX transceivers at the same time, in the experimental setup described hereinafter this architecture has been split into two ML605 evaluation boards (both with external clock sources), we can have two SMA ports with GTX transceivers available at the same time and generate the two signals necessary in the dual comb. In this way, the architecture implemented on both boards (FPGA1 and FPGA2) is the same, except for the IP address for Ethernet communication. Fig. 6 shows this experimental setup and configuration.

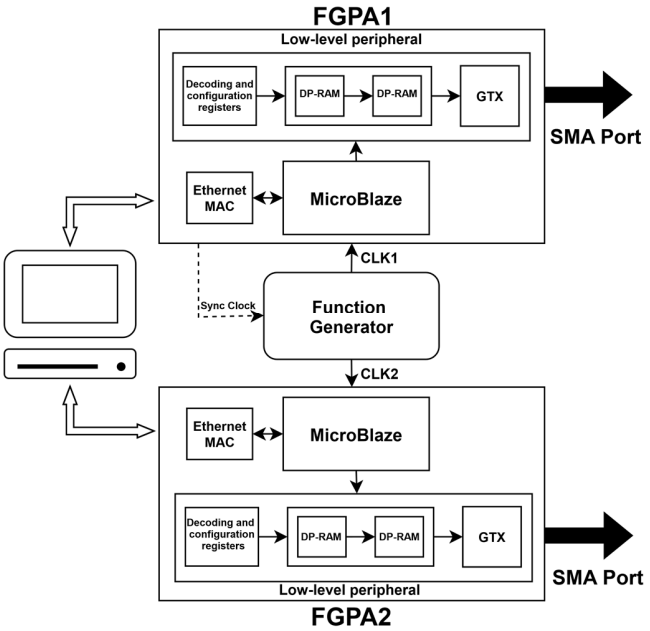

Fig. 6. Experimental setup using two ML605 boards and an external CLK for the PRBS generation.

On the other hand, the dual comb spectroscopy setup is shown in Fig. 7. As previously mentioned, this technique uses two OFCs to produce a frequency downconversion in the optical traces. The role of the FPGAs proposed in this work is to provide the electrical signal that modulates the light source, thus, generating the desired combs. The light source is a distributed feedback fiber laser module (NKT Koheras Basik E15), emitting at 1545 nm to match the sample's absorption peak. The continuous wave signal is divided into two branches by a 90:10 optical coupler (OC) to generate the probe and the LO, respectively. In order to carry out the downconversion process effectively while using both sidebands of the modulated comb, an acousto-optic frequency shifter (AOFS) is positioned in the optical path of the probe comb (as explained in Section II). The signal in the two branches goes through the Mach-Zehnder intensity modulators (MZM), driven the PRBS signals generated as described in Section III. Then, the two signals are amplified and the probe is sent to the sample of interest, in this case, a $H^{13}C^{14}N$ gas cell. Both signals are then band-pass filtered, in order to only keep the first lobe of the PRBS spectra and avoid aliasing between neighboring Nyquist zones. Once filtered, the signals are mixed and sent to a balanced photodiode. The electrical signal is captured by the oscilloscope.

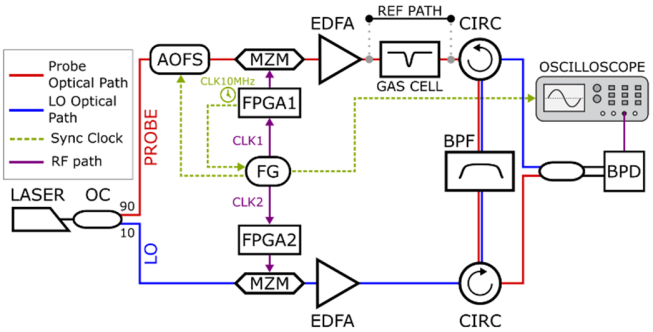

Fig. 7. Scheme of the experimental set-up. OC: optical coupler; AOFS: acousto-optic frequency shifter; MZM: Mach-Zehnder modulator; EDFA: erbium doped fiber amplifier; BPF: band-pass filter; BPD: balanced photodiode; CIRC: circulator.

The 10 MHz reference clock (CLK10MHz) generated by FPGA1 is sent to the frequency generator (FG) and locked with the AOFS and the oscilloscope. The FG feeds the FPGAs with the desired clock frequency, taking into account the 32 multiplying factor ($CLK1 = 156\,007\,500$ Hz and $CLK2 = 156\,023\,484.375$ Hz), so that a dual comb is generated with $N = 1023$ lines in baseband, line spacing $f_R = 4.88$ MHz and offset $\delta f = 500$ Hz. This means that the FPGAs generates PRBS-10 sequences with a bandwidth of $BW = 4.99224$ GHz, which is just below the performance limit of the FPGA.

The frequency shift made by the AOFS has to be chosen so that $f_{AOFS} = k \cdot f_R + f_{NZ}$, with k being a natural number and f_{NZ} being the target central frequency of the downconverted RF comb. In this case, f_{NZ} is chosen to be the center of the first Nyquist Zone in detection. Since the optimal AOFS performance is near 80 MHz, we choose $k = 16$ and $f_{NZ} = 1$ MHz, with the small drawback of losing 16 lines.

The acquired signals are 1 s long, digitalized at 20 Msps. Since $\delta f = 500$ Hz, 500 interferograms (IGMs) are captured in total. Fig. 8 shows the power spectral density (PSD) of the whole 1-s signals (reference and gas cell in blue and orange line, respectively). The spectra show the two downconverted combs in the RF domain. Due to the weak absorption of the gas cell, the two combs are almost identical. The comb lines with the expected line spacing of 500 Hz can be observed in the first inset, showing an SNR of more than 60 dB. The second inset focuses on the center of the Nyquist zone, where the two carriers are shifted 16 lines, as expected from the use of AOFS.

The transmission spectrum of the cell gas is retrieved by comparing the spectrum of the two combs, i.e., with and without the gas cell (using the reference path). For this purpose, the whole 1-s signal is divided into packs of 10 IGMs. In this way, the long-term instabilities of the sync clock are avoided. The 10 IGMs are averaged and the spectrum is obtained by means of a Fourier analysis. All these spectra are then averaged again. To reconstruct the absorption peak of the sample with the correct width, we have to rescale the RF axis by a factor of $f_R/\delta f = 9760$. Thus, we reconstruct the spectral response of the sample with the given spectrometer accuracy, namely, f_R. Fig. 9 shows the experimental points retrieved (in blue) that build the transmission spectrum of the gas cell over 5 GHz of optical bandwidth. The absorption line can clearly be observed. The continuous red line shows a Voigt profile fit. The residuals between the theoretical and experimental points are shown below, having a RMS lower than 2%.

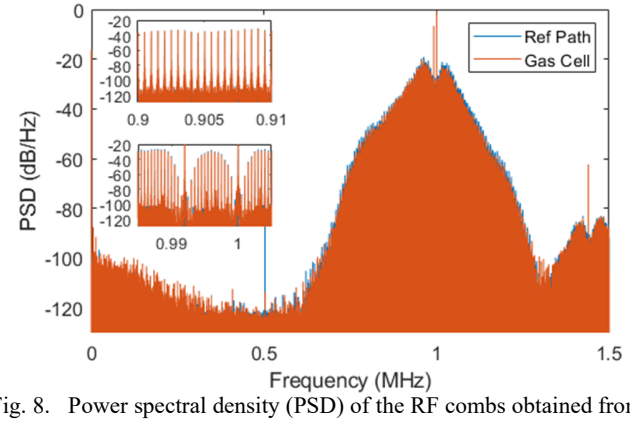

Fig. 8. Power spectral density (PSD) of the RF combs obtained from the 1-s signals corresponding to the reference comb and the probe comb after passing through the gas cell. The first inset shows the comb lines in detail. The second inset provides a detail of the central region of the comb spectrum, where two lines separated by 16 lines are shown due to the effect of the AOFS.

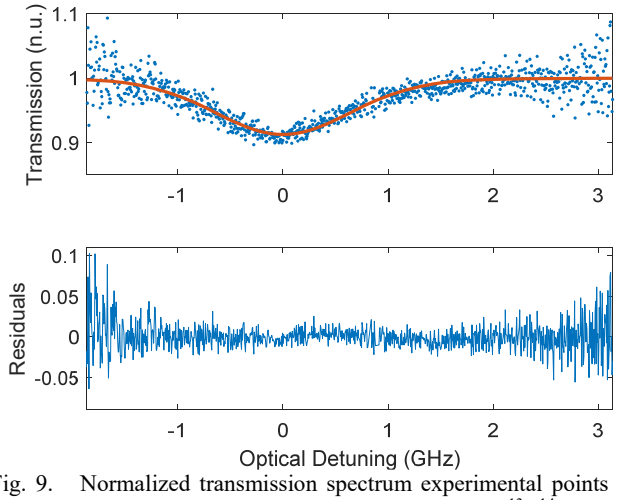

Fig. 9. Normalized transmission spectrum experimental points (in blue dots) showing the P10 absorption line for the $H^{13}C^{14}N$ gas. A Voigt profile fit is shown in blue and the residuals are shown below.

The spectral phase of an absorption peak with such a low depth has a relatively smooth profile (0.12 rad peak-to-peak as estimated by the Kramer-Kronig relation [37]). The spectral phase noise associated to our optical scheme and to the EO comb generation has a standard deviation of 0.2 rad, hindering the proper phase estimation of the detected absorption peak.

V. Conclusions

This work has presented a SoC architecture based on a FPGA device, capable of generating two PRBS sequences and transmitting them at a bit rate in the range of GHz. The proposed architecture is flexible enough to support the run-time reconfiguration of the PRBS sequences, as well as some parameters such as the PRBS length, the pulse width, or sequence peak-to-peak voltage. For that purpose, the architecture includes a Microblaze processor, responsible for

the management of the system and the Ethernet link, used to receive new configurations and set them up. Furthermore, a specific peripheral has been designed to deal with the GTX transceivers, tackling the different clock domains, and, finally, implement the transmission of the PRBS sequences at GHz bit rates. The proposal has been successfully validated on a Virtex6 XC6VLX240T FPGA, where a dual comb spectroscopy measurement has been carried out, targeting a line spacing detuning of the involved combs of 500 Hz. This has allowed to experimentally characterize the absorption peak of a hydrogen cyanide (HCN) gas cell, thus proving the suitability of the proposed architecture for its use in optical spectroscopy. The obtained results allow to foresee the applicability of the proposed solution in a wide variety of fields, such as distributed fiber-optic sensing or LIDAR.

ACKNOWLEDGEMENTS

The authors acknowledge Dr. Vicente Durán for providing the HCN gas cell sample and the laser used in the experimental test.

REFERENCES

[1] M. Pirchi, G. Ziv, I. Riven, S. S. Cohen, N. Zohar, Y. Barak and G. Haran, "Single-molecule fluorescence spectroscopy maps the folding landscape of a large protein", *Nat. Commun.*, vol. 2, no. 493, pp. 1-7, 2011.

[2] F. Shi, F. Kong, P. Zhao, et al. "Single-DNA electron spin resonance spectroscopy in aqueous solutions", *Nat Methods*, vol. 15, no. 493, pp. 697-699, 2011.

[3] C. Slavov, H. Hartmann and J. Wachtveitl, "Implementation and evaluation of data analysis strategies for time-resolved optical spectroscopy", *Anal. Chem.*, vol. 87, no. 4, pp. 2328-2336, Jan. 2015.

[4] Y. Wang, G. M. Ma, D. Zheng, J. Jiang and C. Yan, "Gas concentration sensing based on fiber loop ring-down spectroscopy: a review", *IEEE Trans. Instrum. Meas.*, vol. 70, no. 9509316, pp. 1-16, 2021.

[5] S. Reuter, J. S. Sousa, G. D. Stancu and J. P. Hubertus van Helden, "Review on VUV to MIR absorption spectroscopy of atmospheric pressure plasma jets", *Plasma Sources Sci Technol.*, vol. 24, no. 5, pp. 1-41, 2015.

[6] X. Guo, F. Zheng, C. Li, X. Yang, N. Li, S. Liu, J. Wei, X. Qiu and Q. He, "A portable sensor for in-situ measurement of ammonia based on near-infrared laser absorption spectroscopy", *Opt. Lasers Eng.*, vol. 115, pp. 243-248, 2019.

[7] Y. Yang, Y. Wen, Z. He and J. Zhao, "Optical absorption COD sensor for real-time, low-power-consumption, long-term monitoring", *IEEE Trans. Instrum. Meas.*, vol. 72, no. 9502607, pp. 1-7, 2023.

[8] T. Udem, R. Holzwarth and T. Hänsch, "Optical frequency metrology", *Nature*, vol. 416, pp. 233–237, 2002.

[9] T.J. Kippenberg, R. Holzwarth and S.A. Didddams, "Microresonator-based optical frequency combs", *Science*, vol. 332, pp. 555-559, 2011.

[10] I. Coddington, N. Newbury and W. Swann, "Dual comb spectroscopy", *Optica*, vol. 3, no. 4, pp. 414-426, 2016.

[11] A. J. Fleisher, D. A. Long, Z. D. Reed, J. T. Hodges and F. Plusquellic, "Coherent cavity-enhanced dual-comb spectroscopy", *Opt. Express*, vol. 24, no. 10, pp. 10424–10434, 2016.

[12] J. Nürnberg, B. Willenberg, C. R. Phillips and U. Keller, "Dual-comb ranging with frequency combs from single cavity free-running laser oscillators", *Opt. Express*, vol. 29, no. 16, pp. 24910-24918, 2021.

[13] A. Lukashchuk, J. Riemensberger, M. Karpov, J. Liu and T. J. Kippenberg, "Dual chirped microcomb based parallel ranging at megapixel-line rates", *Nat Commun.*, vol. 13, no. 3280, pp. 1-8, 2022.

[14] B. Martin, P. Feneyrou, D. Dolfi and A. Martin, "Performance and limitations of dual comb based ranging systems", Optics Express, vol. 30, no. 3, pp. 4005–4016, 2022

[15] E. L. Teleanu, V. Durán and V. Torres-Company, "Electro-optic dual-comb interferometer for high-speed vibrometry", Optics Express, vol. 25, no. 14, pp. 16427-16436, 2017.

[16] O. P. Lay, S. Dubovitsky, R. D. Peters, J. P. Burger, S.-W. Ahn, W. H.Steier, H. R. Fetterman and Y. Chang, "MSTAR: a submicrometer absolute metrology system", Opt. Lett., vol. 28, no. 11, p.p. 890-892, 2003.

[17] F. Ferdous, D. E. Leaird, C.-B. Huang and A. M. Weiner, "Dual-comb electric field cross-correlation technique for optical arbitrary waveform characterization", Opt. Lett., vol. 34, no. 24, p.p. 3875-3877, 2009.

[18] X. Zhao, J. Yang, J. Lui, H. Shao, X. Zhang, Q. Li and Z. Zheng, "Dynamic Quasi-Distributed Ultraweak Fiber Bragg Grating Array Sensing Enabled by Depth-Resolved Dual-Comb Spectroscopy", *IEEE Trans. Instrum. Meas.*, vol. 69, no. 8, pp. 5821-5827, 2020.

[19] M. Soriano-Amat, H. F. Martins, V. Durán, L. Costa, S. Martin-Lopez, M. Gonzalez-Herraez and M. R. Fernández-Ruiz, "Time-expanded phase-sensitive optical time-domain reflectometry", *Light Sci. Appl.*, vol. 10, no. 51, pp. 1-12, 2021.

[20] E. Vicentini, Z. Wang, K. Van Gasse, T. W. Hangsch and N. Picqué, "Dual-comb hyperspectral digital holography", *Nature Photon.*, vol. 15, pp. 890-894, 2021.

[21] H. Zhang, L. Xu, Y. Pang and Z. Cao, "Gas Temperature Measurement by Aligning Absorption Spectroscopy of Dual-Phase-Unlocked Optical Combs", *IEEE Trans. Instrum. Meas.*, vol. 71, no. 7005910, pp. 1-10, 2022.

[22] V. Durán, L. Djevarhidjian and H. G. de Chatellus, "Bidirectional frequency-shifting loop for dual-comb spectroscopy", *Opt. Lett.*, vol. 44, no. 15, pp. 3789–3792, 2019.

[23] C. Quevedo-Galán, V. Durán, A. Rosado, A. Pérez-Serrano, J. M. G. Tijero and I. Esquivias, "Gain-switched semiconductor lasers with pulsed excitation and optical injection for dual-comb spectroscopy", *Opt. Express*, vol. 28, no. 22, pp. 33307–33317, 2020.

[24] V. Torres-Company and A. M. Weiner, "Optical frequency comb technology for ultra-broadband radio-frequency photonics", *Laser Photon. Rev.*, vol. 8, no. 3, pp. 368–393, 2013.

[25] A. Parriaux, K. Hammani and G. Millot, "Electro-optic frequency combs", *Adv. Opt. Photonics*, vol. 12, no. 1, pp. 223–287, 2020.

[26] J. Preciado-Garbayo, M. Soriano-Amat, P. Sevillano, D. Izquierdo, H. F. Martins, S. Martin- Lopez, M. Gonzalez-Herraez, M. R. Fernández-Ruiz and J. J. Martínez, "Time-Expanded-OTDR based on binary sequences", *IEEE Photon. Technol. Lett.*, vol. 34, no. 13, pp. 695–698, 2022.

[27] D. V. Sarwate and M. B. Pursley, "Cross correlation properties of pseudorandom and related sequences", *Proceedings of the IEEE*, vol. 68, no. 5, pp. 593-619, 1980.

[28] K. D. Wagner, C. K., Chin and E. J. McCluskey, "Pseudorandom Testing", *IEEE Trans. Comput.*, vol. C-36, no. 3, pp. 332-343, 1987.

[29] K. Fdil, V. Michaud-Belleau, N. Bourbeau Hébert, P. Guay, A. J. Fleisher, J. D. Deschênes and J. Genest, "Dual electro-optic frequency comb spectroscopy using pseudo-random modulation", *Opt. Lett.*, vol., 44, no. 17, pp. 4415-4418, 2019.

[30] J. Preciado-Garbayo, M. Soriano-Amat, P. Sevillano, D. Izquierdo, H. F. Martins, S. Martin-Lopez, M. Gonzalez-Herraez, M. R. Fernández-Ruiz and Juan J. Martínez, "Integrable Architecture for Time expanded Phase-sensitive OTDR based on PRBS", in *27th International Conference on Optical Fiber Sensors*, pp. 1-4, 2022.

[31] H. Tian, S. Fernando, H. Wei Soon, Y. Ha and N. Chen, "Design of a high speed pseudo-random bit sequence based time resolved single photon counter on FPGA", in *2008 International Conference on Field Programmable Logic and Applications (FPL)*, pp. 583-586, 2008.

[32] "NIST, SRM 2519a." [Online]. Available: https://www-s.nist.gov/srmors/view_detail.cfm?srm=2519A.

[33] Xilinx, Inc., *MicroBlaze Processor Reference Guide*, UG984, 2022.

[34] Xilinx, Inc., *Virtex-6 FPGA GTX Transceivers*, User Guide, UG366, 2011.

[35] Xilinx, Inc., *Virtex-6 FPGA Clocking Resources*, User Guide, UG362, 2014.

[36] Xilinx, Inc., *Virtex-6 Family Overview*, Product Specification, DS150, 2015.

[37] A. V. Oppenheim and R. W. Schafer, *Discrete-Time Signal Processing*, Prentice-Hall, New Jersey, 2nd edition, 1989.

Miguel Tapiador received his Bachelor's Degree in Electronic Communications Engineering, and his Master's Degree in Electronics Engineering by the University of Alcalá (UAH), Spain, in 2021 and 2022, respectively. He is currently a PhD candidate at the Electronics Department from the University of Alcala. His research activities are focused on developing digital systems, mainly on FPGA devices, for different purposes such as photonics and ML systems.

Camilo Escobar-Vera received his bachelor's degree in Physics by the University of Valladolid in 2019 and the M.Sc. in Laser Physics from the University of Salamanca in 2021. He is currently a Ph.D. student in the Photonics Engineering Group at the University of Alcalá, Spain. His research is focused on distributed fiber sensors based on optical frequency combs.

Miguel Soriano-Amat received the bachelor's degree in Physics and the master's degrees in Advanced Physics from the Universitat de València, Valencia, Spain, in 2017 and 2018, respectively. He is currently a Ph.D. student in the Photonics Engineering Group at the University of Alcala, Spain. His research activities are focused on the developing of high-resolution distributed acoustic sensors based on optical frequency combs.

Sonia Martin-Lopez (Member, IEEE), received the Ph.D. degree from the Universidad Complutense de Madrid, Madrid, Spain, in May 2006. She had a Predoctoral stay with the Nanophotonics and Metrology Laboratory, Ecole Polytechnique Federale de Lausanne, Lausanne, Switzerland. She has been involved as a Postdoctoral Researcher with Applied Physics Institute and with the Optics Institute, Spanish Council for Research for six years. She is currently an Associate Professor with the Photonics Engineering Group, University of Alcala, Spain. She is the Author or Co-Author of more than 200 papers in international refereed journals and conference contributions. Her current research interests include nonlinear fiber optics and distributed optical fiber sensors.

Miguel Gonzalez-Herraez (Senior Member, IEEE), received the D.Eng. in Telecommunications Engineering from Universidad Politécnica de Madrid, Madrid, Spain, in 2004. Since 2004, he has been with the Department of Electronics, University of Alcala, Madrid, Spain, where he is currently a Full Professor. He is the author or coauthor of more than 300 research articles in indexed journals and contributions to prestigious international conferences in the field of photonics. His current research interests include distributed optical fiber sensing, nonlinear fiber optics, and ultrafast fiber lasers. He is an Associate Editor for the IEEE Photonics Technology Letters, and a Senior Member of the Optical Society of America.

Álvaro Hernández (Senior Member, IEEE), received the Ph.D. degree from the University of Alcala, Spain, and from Blaise Pascal University, France, in 2003. He is currently a Professor of digital systems and electronic design with the Electronics Department, University of Alcala. His research areas are multisensory integration, electronic systems, and digital and embedded systems.

María R. Fernández-Ruiz received the M.Eng. in Telecommunications and M.Sc. in Electronics and Signal Processing from the University of Seville, Spain, in 2009 and 2011, respectively, and the Ph.D. degree in Telecommunications from the University of Quebec, Montreal, Canada, in 2016. She is currently a Ramon y Cajal Postdoctoral Researcher with the Photonics Engineering Group, University of Alcala, Spain. Her research focuses on the development of new architectures and applications for distributed acoustic sensor systems. She is the author or co-Author of more than 100 papers in international refereed journals and conference contributions. Her current research interests include optical signal processors, nonlinear optics, and distributed optical sensors.